

Article

Functionalized TiO₂ Nanotube Platform for Gliadin Electroanalysis

Cristina Dumitriu, Alexandra Constantinescu and Cristian Pirvu *

General Chemistry Department, Faculty of Applied Chemistry and Materials Science, University Politehnica of Bucharest, 313 Splaiul Independentei, 060042 Bucharest, Romania; dumitriu.cristina.o@gmail.com (C.D.); aconstantinescu3108@stud.fim.upb.ro (A.C.)

* Correspondence: c_pirvu@chim.pub.ro or c_pirvu@yahoo.com; Tel.: +40-214023930

Abstract: The present paper presents a gliadin detection method. This method is based on a modified Ti electrode. Modification was performed by a simple and cheap anodization. Then, a layer of graphene oxide was added, and gliadin antibody was fixed on the electrode surface. Using this complex system, electrochemical impedance spectroscopy was used for gliadin detection. Solutions with known gliadin (a fraction from gluten) content were used for analysis. Impedance measured at a certain frequency and coating resistance were analyzed. Better results (good linearity and lower detection limit) were obtained by plotting impedance at a certain frequency versus gliadin concentration. Coating resistance was proved to be in linear dependency with gliadin concentration only at lower concentrations. This system based on titanium nanostructured electrode has the potential to be used for gluten contamination detection from foods.

Keywords: titanium dioxide nanotubes; electrochemical methods; gliadin detection



Citation: Dumitriu, C.; Constantinescu, A.; Pirvu, C. Functionalized TiO₂ Nanotube Platform for Gliadin Electroanalysis. *Crystals* **2021**, *11*, 22. <https://doi.org/10.3390/cryst11010022>

Received: 2 December 2020

Accepted: 24 December 2020

Published: 29 December 2020

Publisher's Note: MDPI stays neutral with regard to jurisdictional claims in published maps and institutional affiliations.



Copyright: © 2020 by the authors. Licensee MDPI, Basel, Switzerland. This article is an open access article distributed under the terms and conditions of the Creative Commons Attribution (CC BY) license (<https://creativecommons.org/licenses/by/4.0/>).

1. Introduction

Celiac disease is a well-known chronic immune-mediated disorder initiated by dietary gluten, having a prevalence of approximately 1% worldwide [1–3]. Although research is being done, a life-long gluten-free diet, first treatment from more than a half-century, remains the only treatment currently recognized [3,4]. For celiac disease patients, adherence to a gluten-free diet prevents further complications. There also some other related gluten disorders in which adherence to a gluten-free diet is required [5,6].

Different cereals like wheat, barley, oats, rye or their crossbred varieties contain gluten [7]. Gluten has two subfractions: gliadins, single-chain proteins soluble in alcohol-water mixture and glutenin, insoluble poly-peptide chain macromolecules [2,8].

Food products can be labeled as “gluten-free” if their gluten content is <20 ppm (20 mg/kg product) and as “very low gluten content” if the gluten content is in [1,9] the range 20–100 ppm [1,9,10]. A common method is using the sandwich ELISA test kit based on R5 and Skerrit antibodies. However, this method has some disadvantages: it cannot identify the source of gluten—whether it is from wheat, rye, or barley; it takes a long time (between 30 min and 2.5 h depending on the manufacturer); it has difficulties in testing the heat-processed food samples (especially glutenin) [11,12]. R5 sandwich ELISA cannot be applied for hydrolyzed protein products, so R5 competitive ELISA, ELISA G12, and mass spectrometry was developed for hydrolyzed food [7]. Given these problems, other different methods were developed. One method is a genomic method—PCR (polymerase chain reaction) using specific DNA sequences [12,13]. A double PCR system was developed with DNA isolated from different cereals. First, genomic eukaryote DNA sequences were used to prove isolated nucleic acid substrate accessibility to PCR amplification. Then a wheat genomic DNA segment was amplified by PCR for wheat detection. DNA samples only are screened for wheat genomic DNA when the tested sample has proved positive for the first test [13]. It is much more sensitive compared to ELISA and can distinguish the source of

gluten or cereal proteins but cannot be applied to the hydrolyzed proteins either [11,12]. Moreover, non-immunological matrix-assisted laser desorption/ionization time-of-flight mass spectrometry (MALDI-TOF MS) was applied for gluten detection with high sensitivity but with high costs and specialized equipment. Chromatographic techniques like: HPLC coupled to mass spectrometry (LC-MS/MS), gel permeation (GP) chromatography, reverse-phase (RP) chromatography, have also been used to detect gluten [12]. Another group of methods applied for this allergen detection are optical methods: near-infrared (NIR) [12] or recently luminescent sensing based on phosphorescent switch-on probe [14]. Many of these mentioned methods are using expensive equipment and considerable sample/reagent consumption, require complicated sample pre-treatment and are time-consuming [14].

Recently, electrochemical methods were also used for gluten detection from food or human samples—amperometry [15–17], surface plasmon resonance (SPR) [18], impedance [19], voltammetry [20,21]. Amperometric methods have used aptamers in different approaches. In two studies, aptamers were immobilized onto the surface of streptavidin-modified magnetic particles on carbon screen printed electrodes to allow chronoamperometric detection of gluten from different foods, including treated ones (heat-treated and hydrolyzed) [15,17]. Amperometric flow system was used with an immunodominant peptide from gliadin coupled to a competitive ELISA. A reduction of the enzymatic reaction time was obtained, and the results were well correlated with optical measurements [16]. Antibody was linked on gold SPR electrode via self-assembled monolayer (SAM) and it was used for gluten detection from patients' urine samples [18]. A sensor based on electrochemical impedance spectrometry also used aptamers immobilized on gold working electrode using poly (amidoamine) dendrimers [19]. Voltametric methods were based on differential pulsed voltammetry (DPV). One study used reduced graphene oxide modified electrodes with antibodies [21] and the other just a pencil graphite unmodified electrode [20].

Graphene oxide (GO) was used for sensor applications because of very good charge transfer capabilities, and because it can serve as supporting layers for biomolecules and presents high surface-to-volume ratio and low electrical noise [22]. Graphene oxide was already used for sensing gliadin (component of gluten) [21]. In another study, our group also used Ti electrode with graphene oxide deposited using cyclic voltammetry to test gluten presence [9].

Titanium dioxide (TiO₂) nanoparticles and nanotubes were used for example in constructing a glucose, cholesterol, or cancer cells sensor [22–24]. They were used in sensors applications because they can be easily prepared with high reproducibility and low cost, they have a large surface area and they are non-toxic, hydrophilic, and biocompatible [22,24]. These nanostructures have also other important characteristics: they have antibacterial activities, confer UV protection [25], and have the ability to incorporate compounds for controlled release [26].

Several studies combined these two nanomaterials—TiO₂ nanotubes and graphene oxide for sensors applications, to overcome the disadvantages of each of them and benefit from their advantages [22].

In this study, combined TiO₂ nanotubes—graphene oxide antigliadin antibody was tested for gluten presence evaluation. An electrochemical method was used—electrochemical impedance spectroscopy at open circuit potential. Two result interpretations were analyzed: impedance at a certain frequency versus gliadin concentration and coating resistance obtained by fitting the results versus gliadin concentrations.

2. Materials and Methods

Titanium round bars with 8 mm diameter (99.99% purity, Alpha Aesar) were cut into small pieces (3 mm thick). Pieces were polished using a Beta 2 grinder-polisher with CarbiMet (Buehler) abrasive papers, having porosities from 800 to 1200. Then, to remove impurities and obtain degreasing/pickling, samples were immersed in the ultrasound bath (model Ti-H-5 from Transsonic) for 15 minutes in distilled water, ethanol, and then acetone.

After samples were dried at room temperature, they were mounted in Origalys system to have a controlled surface.

TiNT were prepared by 2 hours' anodization at room temperature in ethylene glycol (Chimreactiv, anhydrous, 99.8% purity) with 0.5% w NH₄F (Sigma Aldrich) and 2% distilled water. A spiral platinum wire (model 50SP17, Redox Research & Analytic, Otopeni, Romania) was used as counter electrode. Electrolysis was performed with an MPS-7163 (MATRIX) power source, at 50 V. After anodization, the sample was rinsed with distilled water to remove any electrolyte remains and was subjected to thermal treatment, 4 h at 400 °C in air, using an LEF-1035 (Daihan Labtech, Gyeonggi-do, Republic of Korea) oven.

TiNT GO was prepared by depositing graphene oxide (GO) using cyclic voltammetry 30 cycles between −1.5 and 1.0 V, with 40 mV/s scan rate. Deposition was performed using an Autolab potentiostat/galvanostat model 302 N (Metrohm). A three-electrode system was used: TiNT working electrode, platinum rod (Metrohm) counter electrode, and Ag/AgCl 3 M KCl reference electrode (Metrohm). Electrolyte was 0.5 mg/mL graphene oxide (powder, 15–20 sheets, 4–10% edge-oxidized, Sigma Aldrich) in 0.1 M phosphate buffer pH 9.3. Buffer was made from 0.2 M aqueous stock solutions of Na₂HPO₄ and NaH₂PO₄ (Sigma Aldrich) and NaOH (Sigma Aldrich) 0.1 M.

TiNT GO anti-gliadin antibody was prepared in several steps, all at room temperature and light, each in sterile containers. In the first step, TiNT GO was immersed in 1 mM aqueous solution of 1-pyrenecarboxylic acid (Sigma Aldrich). After 1 hour, samples were rinsed with distilled water and then immersed another half an hour in a mixture of 15 mM N-(3-dimethylaminopropyl)-N'-ethylcarbodiimide hydrochloride (EDC, Sigma Aldrich)/15 mM N-hydroxysuccinimide (NHS, Sigma Aldrich) in 0.1 M phosphate buffer pH 7.4 (made from 0.2 M stock aqueous solutions of Na₂HPO₄ and NaH₂PO₄ from Sigma Aldrich). Two drops of 7 microliters each from a buffered aqueous solution of anti-gliadin (wheat) antibody produced in rabbit (Sigma Aldrich) were added using a Gilson micropipette on electrode surface. After 40 minutes, the electrode was rinsed with phosphate buffer. The final step was immersion in 2 w/v % bovine serum albumin (BSA, Sigma Aldrich) in phosphate buffer pH 7.0. After 1 hour, TiNT GO antibody was rinsed with phosphate buffer and allowed to dry.

Samples were characterized using surface electron microscopy (SEM, FEI Quanta 650 FEG – Thermo Fisher Scientific, Waltham, MA, USA) at different magnifications.

Contact angle was measured with distilled water at room temperature and light using sessile drop method, with a CAM 100 contact angle meter (KSV Instruments LTD). A small drop was deposited from a Pyrex glass syringe with a blunt tip needle. Five measurements were performed on each sample.

Four consecutive scans of infrared spectra were recorded with a Fourier transform (FT-IR) Spectrum 100 (Perkin Elmer, Shelton, CT, USA), between 4000 and 600 cm^{−1}, after each step.

Atomic force microscopy images were recorded with a machine from APE Research, Italy and processed with Gwyddion 2.9 software (A.P.E. Research srl, Trieste - Italy).

Electrochemical impedance spectroscopy measurements were performed with three electrode system using Autolab 302N (Metrohm, Eco Chemie, Utrecht, The Netherlands) with Nova 1.11 software. Measurements were performed in buffer solutions pH 7. Impedance spectra were recorded between 0.1–10⁵ Hz, with 0.01 amplitude at open circuit potential. Only obtained experimental points between 0.1 and 5963 Hz were fitted using Nova 1.11 software (Metrohm, Nova 1.11, Eco Chemie, Utrecht, The Netherlands).

To avoid contaminations, sterile containers were used as electrochemical cell. Between measurements, electrodes were rinsed. Before recording a spectrum in a solution with gliadin, the working electrode was let in contact 30 min in this solution, to allow antibody–antigen coupling. For working electrode regeneration between measurements, a solution of NaOH/H₃PO₄, pH = 12, was used. Gliadin standard solutions were prepared using alcohol 60% and phosphate buffer.

3. Results

The scheme of titanium electrode modification with nanotubes, graphene oxide, and gliadin antibody are presented in Figure 1.

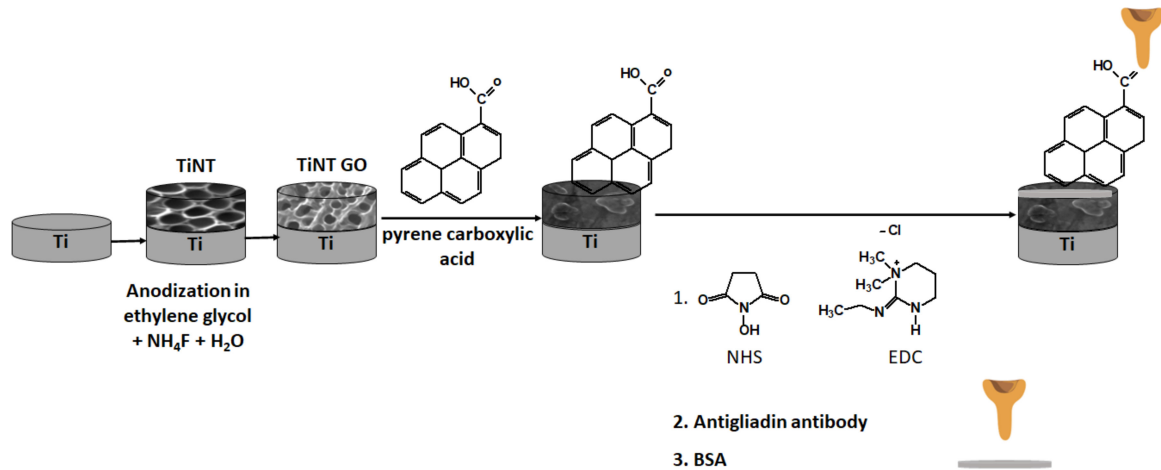


Figure 1. Nanostructured titanium modified with graphene oxide and antibody.

Nanotubes were created because they allowed a higher surface. They were subjected to thermal treatment to increase crystallinity.

GO was deposited to increase the conductivity. It also increases the specific surface, allowing a high amount of antibody to be immobilized. It is also mentioned in literature that GO promotes diffusion of the analyte through interconnected pores [21].

Pyrene carboxylic acid was added to allow covalent bond with antigliadin antibody thru NHS and EDC chemistry.

Gliadin antibody was used to render the electrode specificity for gliadin (a gluten fraction).

In Figure 2a, Origalys system is presented. The Origalys system allowed a controlled surface, which is very important in electrochemical experiments. System design allowed round-shaped samples. It was used for all experiments. During thermal treatment, the samples were removed easily. For GO deposition and antibody deposition, the sample remained in the Origalys system.

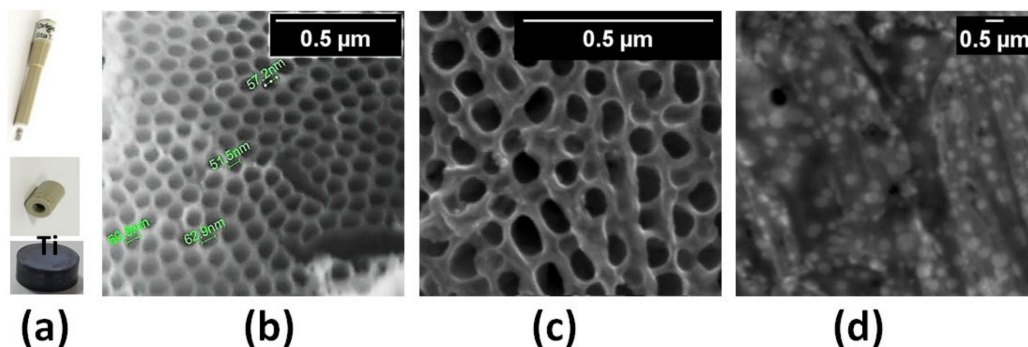


Figure 2. Origalys system with Ti electrode used in this study (a) and top view SEM images after each modification step: TiNT (b), TiNT GO (c), TiNT GO antibody (d).

After each modification step, the sample morphology was changed from thin-walled nanotubes (Figure 2b), to nanotubes having thick walls (Figure 2c) after GO addition. After all steps for antibody immobilization (presented in Figure 1), partially covered nanotubes were obtained (Figure 2d).

In Figure 3, contact angle and Atomic Force Microscopy images are shown for Ti and modified samples. Contact angle values presented in the image are the average values of five measurements.

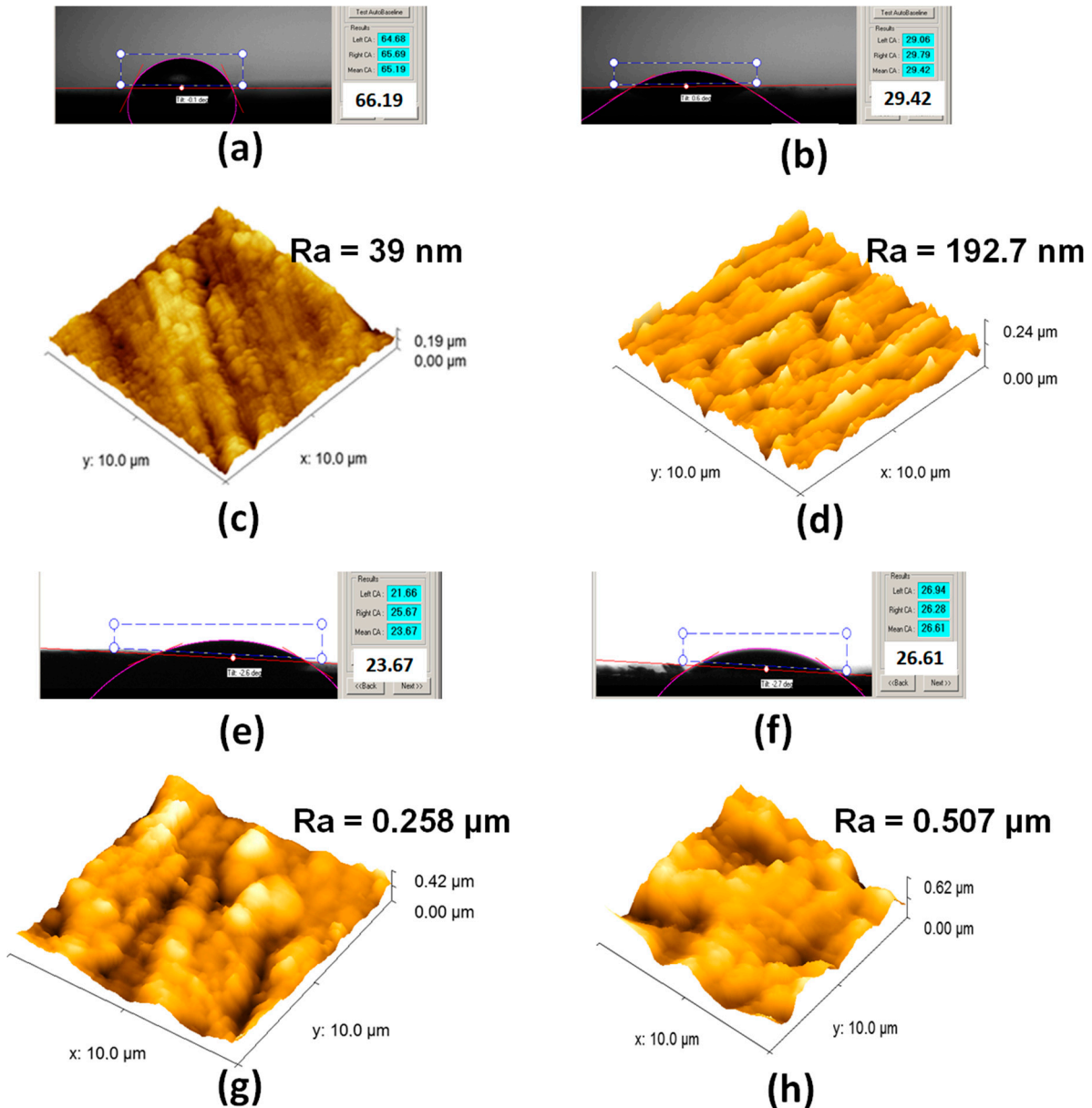


Figure 3. Average contact angle and 3D AFM images with obtained Ra values for: (a,c)—Ti, (b,d)—TiNT, (e,g)—TiNT GO, (f,h)—TiNT GO antibody.

The software for contact angle measuring device, gave left, right, and mean value for each measurement. The mean value of five different consecutive measurements for each of four samples was written in the Excel program. The average (presented in Figure 3) and the standard deviation for water contact angle were calculated for each sample. The standard deviation values were: 1.90 for Ti, 0.69 for Ti NT, 1.14 for TiNT GO, and 0.67 for TiNT GO antibody. The relatively small standard deviation values show that the sample surface is uniform. Ti substrate was freshly polished before contact angle recording.

Comparative FT-IR spectra are presented in Figure 4, after each modification step. They were recorded with 4 cm^{-1} resolution. Four consecutive scans were applied for each sample. Each sample has its own color, the same in all graphs. Using the equipment-

corresponding software, the spectra were processed using background correction and automatic smoothing.

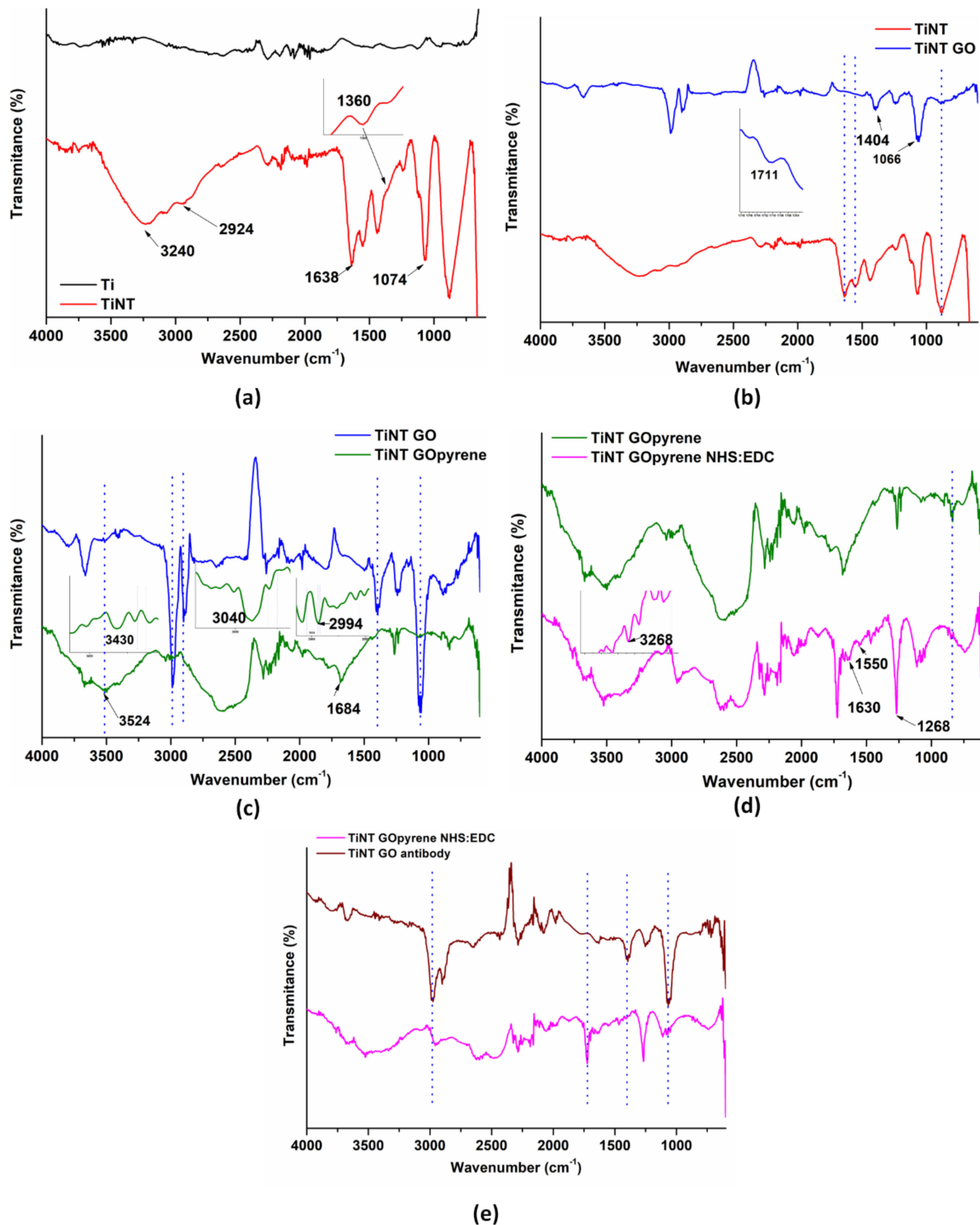


Figure 4. Comparative FT-IR spectra after each modification step: (a) Ti and TiNT, (b) TiNT and TiNT GO, (c) TiNT GO and TiNT GOpyrene, (d) TiNT GOpyrene and TiNT GOpyrene NHS:EDC, (e) TiNT GOpyrene NHS:EDC and TiNT GO antibody.

For the TiNT sample (Figure 4a, red line), C-O-C bond and CH₂ groups at 1360 cm⁻¹ (in inset) and respective at 2924 cm⁻¹ are present, peak at 1638 cm⁻¹ correspond to coordinated H₂O as well as Ti-OH, and C-C stretching appears at 1074 cm⁻¹ [27]. Traces of organic electrolyte remained.

The TiNT GO sample, blue line Figure 4b, has characteristic peaks. The peak at 1711 cm^{-1} it is assigned for C=O stretching, the one at 1404 cm^{-1} for O-H deformation, and C-O stretching appears at 1066 cm^{-1} [28].

When pyrene carboxylic acid was added (Figure 4c, green line), peaks for -COOH group are visible: at -OH in carboxylic acid which form intramolecular bonds at 3524 cm^{-1} and -OH stretching vibration at 3430 cm^{-1} . C=O stretching appears at 1684 cm^{-1} . The C-H stretching vibrations of aromatic and heteroaromatic stretching vibrations appears at 3040 cm^{-1} and 2994 cm^{-1} [29].

After EDC/NHS addition (Figure 4d—magenta line), amide A (N-H stretch coupled with hydrogen bonding) at 3268 cm^{-1} . Additionally, 1630 cm^{-1} corresponds to amide I (CO stretch), 1550 cm^{-1} is assigned to amide II (NH bend coupled with CN stretch), and the sharp peak at 1268 cm^{-1} for amide III (NH bend) [30].

The modified electrode was tested in buffer solutions and buffer solutions containing known gliadin concentrations. The concentrations were selected between 10 and 80 ppm gliadin.

In Figure 5, a Bode modulus diagram is shown for TiNT GO antibody in electrolyte without and with different gliadin concentrations. The obtained signal (impedance) is not proportional to the concentration increase for all tested gliadin concentrations (between 10 and 80 ppm), at all frequencies in 0.1– 10^5 domain.

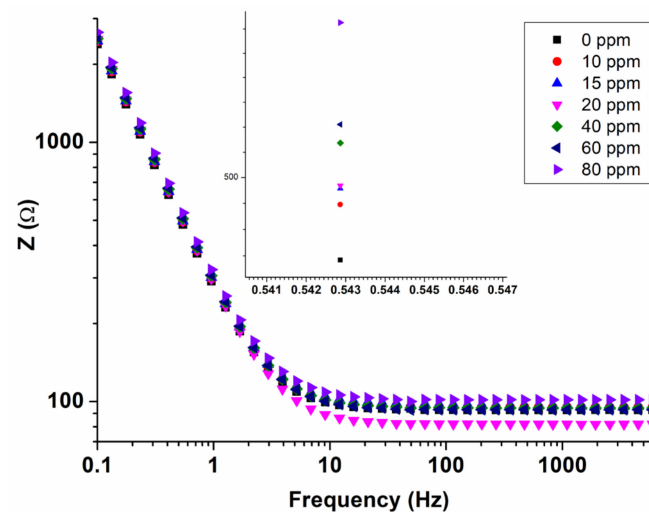


Figure 5. Bode Modulus diagram for modified TiNT GO antibody electrode between 0.1 and 10^5 Hz in phosphate buffer vs. Ag/AgCl 3 MKCl (magnification for 0.543 Hz in the inset).

In this diagram, frequency and impedance (Z) are on a logarithmic scale. In the inset can be seen an increased magnification corresponding to the frequency of 0.543 Hz. Nyquist and Bode phase diagrams are not presented.

To observe signal stability, we recorded three consecutive scans in each concentration. The electrode was carefully rinsed between measurements. For 0.543 Hz, the obtained impedance, at different concentrations, was added in Excel to allow the calculation of the standard deviation. The following standard deviation values were obtained for TiNT GO antibody electrode in phosphate buffer with gliadin: 0.531 in 0 ppm, 3.764 in 10 ppm, 0.808 in 15 ppm, 1.320 in 20 ppm, 2.089 in 40 ppm, and 2.279 in 80 ppm. The standard deviation is highest for 10 ppm gliadin concentration. The difference between the values obtained during three consecutive scans for one concentration is not big, the signal being stable.

In Figure 6, a graph of impedance vs. concentration is presented. It has a linear tendency, the Pearson's R being 0.990. The graph and linear fitting of the data were obtained with Origin software. Only six points were selected.

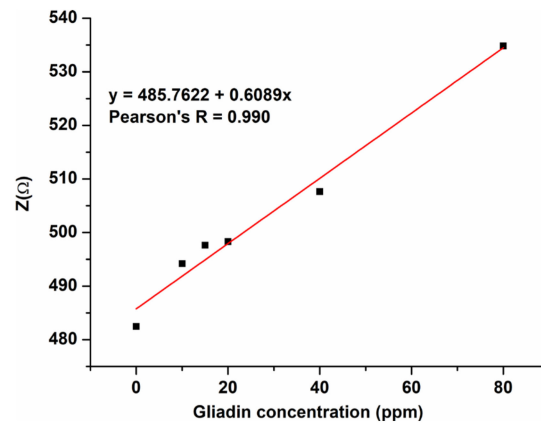


Figure 6. Change of impedance at 0.543 Hz as a function of gliadin concentration for TiNT GO antibody modified electrode in phosphate buffer.

Impedance data were fitted using equivalent circuit from Figure 7a. In this circuit, R_s is the solution resistance. Other resistance was added as R_{coating} for coating layer (barrier oxide + nanotubes + graphene oxide + linker – pyrene carboxylic acid and NHS EDC system + antigliadin antibody) in parallel with CPE. CPE is the constant phase element. CPE has two components: Y and N . The first one is the numerical value of admittance. The second one ranges between 0 and 1. It is an empirical constant. Value 1 indicates a pure capacitor, and value 0, a pure resistor.

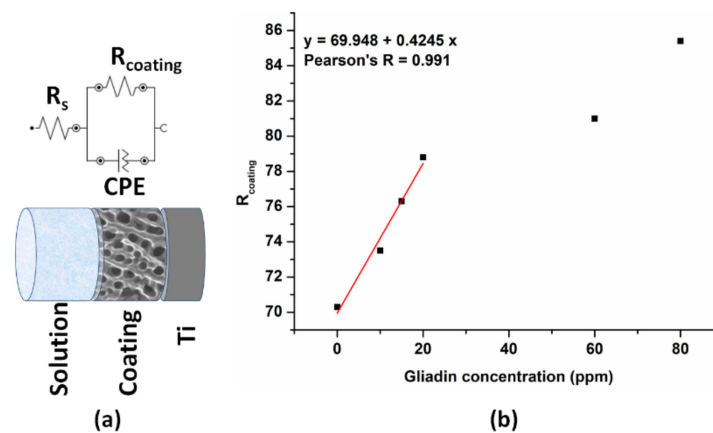


Figure 7. The equivalent circuit used to fit the impedance data and physical attribution to each value (a); R_{coating} vs. gliadin concentration (b).

R_{coating} was plotted against concentration. It has also a linear tendency.

Results from fitting are presented in Table 1 for all seven concentrations, including the values for the two components of constant phase element (CPE).

Table 1. Parameters of equivalent electrical circuits used for fitting the EIS data.

Element	Sample	0 ppm	10 ppm	15 ppm	20 ppm	40 ppm	60 ppm	80 ppm
R_s	$[\Omega]$	92.80	94.97	96.76	81.80	94.40	92.90	101.43
R_{coating}	$[\text{k}\Omega]$	70.3	73.5	76.3	78.8	72.2	81.0	85.4
CPE	$Y_{01}/S \cdot s^{-n}$	$6.53 \cdot 10^{-4}$	$6.38 \cdot 10^{-4}$	$6.35 \cdot 10^{-4}$	$6.26 \cdot 10^{-4}$	$6.20 \cdot 10^{-4}$	$6.14 \cdot 10^{-4}$	$5.88 \cdot 10^{-4}$
	N	0.965	0.965	0.964	0.968	0.967	0.966	0.966
	χ^2	0.011	0.006	0.014	0.007	0.006	0.006	0.016

4. Discussion

The entire electrode modification process presented schematically in Figure 1 has many steps and takes many hours (2 h anodization, 4 h calcination, several minutes GO deposition, 3 h antibody deposition).

In Figure 2b, a very ordered nanotubular layer can be seen, having internal diameters of around 60 nanometers.

It is known that after anodization nanotubes are amorphous. Literature studies show that an increased voltage used for nanotube formation is conducive to an increase of the crystallinity of anodic TiO₂ films [31]. In our case, anodization was performed at a higher voltage (50 V), so nanotubes are expected to have a certain degree of crystallinity. However, thermal treatment is still needed to reach a crystalline phase.

In Figure 2c, after graphene oxide deposition, the nanotubes' walls are much thicker. After the final step, antibody deposition, Figure 2d, the nanotubes' surface is covered. The structure is still porous.

As presented in Figure 3, for untreated Ti, an average contact angle value of 66° was obtained. The substrate is hydrophilic, with a roughness of 39 nm. For TiNT sample, the contact angle value was lower (average 29°), and the roughness was increased from 39 to 192.7 nm. In our case, a hydrophilic substrate, by nano-structuration, becomes more hydrophilic with a higher surface roughness. According to literature [32], this corresponds to Wenzel state.

After GO deposition on titanium dioxide nanotubes, the contact angle is not influenced as much. It remains also close to 20° (Figure 3e), but the roughness is very much increased (Figure 3g). Antiglin antibody deposition does not influence much hydrophilicity (Figure 3f, about 20°) but this sample is the roughest (Figure 3h).

In Figure 4a, a comparison can be seen between Ti and TiNT spectra. Between 3000 and 3500 cm⁻¹, the broad peak is assigned for -OH groups [27]. Other characteristic peaks are visible for the anodized sample. In Figure 4b–d, the appearance or disappearance of some peaks is visible after each step. These peaks are marked with a dotted line.

The used method was impedance spectroscopy because it is a simple method and it disturbs the interface at minimum, measurements being performed at open circuit potential.

To make a calibration curve, the impedance at 0.543 Hz was selected. At this frequency, the impedance is proportional with concentration.

The limit of detection (LOD) and the limit of quantification (LOQ) were determined using linear regression according with method presented in literature [33]. LOD was 14 ppm and LOQ 45 ppm. According to presented literature, a food can be labeled as "gluten-free" if it has gluten content below 20 ppm. So, further work will be necessary to lower LOQ to 20 ppm.

From Figure 7, it can be seen that R_{coating} values are linear only in the 0–20 ppm domain, with Pearson's R of 0.991. After this concentration, it does not have good linearity. In this case, LOD and LOQ were not calculated. It seems to work only for lower concentrations. For many patients with disorders related to gluten, contaminations can be very harmful [5,6].

In this case, a better result was obtained by monitoring the impedance at one frequency than to fit the data and use obtained resistance for a calibration curve.

From Table 1, it can be seen that the solution resistance has similar values for all the samples, as it was expected. N have values around 0.9 in all the cases, indicating a pseudocapacitive behavior. R_{coating} increased when the gliadin concentration was increased, except one case, at 40 ppm.

5. Conclusions

A complex electrode modification was obtained on titanium substrate. This modification is easy to achieve. A cheap method, electrolysis, was used to obtain the nanostructured electrode.

To determine the ability of this system to be used for gluten detection from foods, antigliadin antibody was immobilized on electrode surface using a chemical linker NHS:EDC mixture. It was tested against known concentrations of gliadin using a simple electrochemical method: impedance spectroscopy.

This complex system has the potential to be used for gluten presence evaluation from foods. Future work is necessary to lower LOQ and verify additional parameters required for a sensor. The system works better at lower gliadin concentrations, and could be suitable to verify food contamination, which is a problem for some very sensitive patients.

Author Contributions: Conceptualization, C.D. and C.P.; methodology, C.D., and C.P.; software, C.D. and A.C.; validation, C.D., C.P. and A.C.; formal analysis, C.D. and A.C.; investigation, C.D. and A.C.; resources, C.D.; data curation, C.D.; writing—original draft preparation, C.D.; writing—review and editing, C.D. and C.P.; supervision, C.P.; project administration, C.D.; funding acquisition, C.D. All authors have read and agreed to the published version of the manuscript.

Funding: This research was funded by Romanian Ministry of National Education, through UEFISCDI, grant number PN-III-P1-1.1-PD-2016-2185.

Acknowledgments: The SEM analyses on FEI/Philips XL-30 QUANTA 650 was funded by European Regional Development Fund through Competitiveness Operational Program 2014–2020, Priority axis 1, Project No. P_36_611, MySMIS code 107066, Innovative Technologies for Materials Quality Assurance in Health, Energy and Environmental—Center for Innovative Manufacturing Solutions of Smart Biomaterials and Biomedical Surfaces—INOVABIOMED.

Conflicts of Interest: The authors declare no conflict of interest.

References

1. Xu, J.; Zhang, Y.; Wang, W.; Li, Y. Advanced properties of gluten-free cookies, cakes, and crackers: A review. *Trends Food Sci. Technol.* **2020**, *103*, 200–213. [\[CrossRef\]](#)
2. Rossi, S.; Capobianco, F.; Sabatino, G.; Maurano, F.; Luongo, D.; Rossi, M. Pilot scale production of a non-immunogenic soluble gluten by wheat flour transamidation with applications in food processing for celiac-susceptible people. *J. Cereal Sci.* **2020**. [\[CrossRef\]](#)
3. Gobetti, M.; Pontonio, E.; Filannino, P.; Rizzello, C.G.; De Angelis, M.; Di Cagno, R. How to improve the gluten-free diet: The state of the art from a food science perspective. *Food Res. Int.* **2018**, *110*, 22–32. [\[CrossRef\]](#)
4. Al-Toma, A.; Volta, U.; Auricchio, R.; Castillejo, G.; Sanders, D.S.; Cellier, C.; Mulder, C.J.; Lundin, K.E.A. European Society for the Study of Coeliac Disease (ESsCD) guideline for coeliac disease and other gluten-related disorders. *United Eur. Gastroenterol. J.* **2019**, *7*, 583–613. [\[CrossRef\]](#)
5. Paul, S.P.; Stanton, L.K.; Adams, H.L.; Basude, D. Coeliac disease in children: The need to improve awareness in resource-limited settings. *Sudan J. Paediatr.* **2019**, *19*, 6–13. [\[CrossRef\]](#)
6. Taraghikhah, N.; Ashtari, S.; Asri, N.; Shahbazkhani, B.; Al-Dulaimi, D.; Rostami-Nejad, M.; Rezaei-Tavirani, M.; Razzaghi, M.R.; Zali, M.R. An updated overview of spectrum of gluten-related disorders: Clinical and diagnostic aspects. *BMC Gastroenterol.* **2020**, *20*, 258. [\[CrossRef\]](#)
7. Rai, S.; Kaur, A.; Chopra, C.S. Gluten-Free Products for Celiac Susceptible People. *Front. Nutr.* **2018**, *5*. [\[CrossRef\]](#)
8. Han, C.; Ma, M.; Li, M.; Sun, Q. Further interpretation of the underlying causes of the strengthening effect of alkali on gluten and noodle quality: Studies on gluten, gliadin, and glutenin. *Food Hydrocoll.* **2020**, *103*, 105661. [\[CrossRef\]](#)
9. Dumitriu, C.; Constantinescu, A.; Pirvu, C. Electrochemical platform based on modified ti electrodesto test a food allergen presence. *Rev. Chim.* **2020**, *71*, 427–433. [\[CrossRef\]](#)
10. Panda, R.; Garber, E.A.E. Detection and quantitation of gluten in fermented-hydrolyzed foods by antibody-based methods: Challenges, progress, and a potential path forward. *Front. Nutr.* **2019**, *6*. [\[CrossRef\]](#)
11. Deora, N.S. Current detection and quantification method for gluten to support the gluten-free claim: An insight about elisa method. *J. Nutr. Health Food* **2018**, *8*, 75–76. [\[CrossRef\]](#)
12. Osorio, C.E.; Mejías, J.H.; Rustgi, S. Gluten detection methods and their critical role in assuring safe diets for celiac patients. *Nutrients* **2019**, *11*, 2920. [\[CrossRef\]](#)
13. Allmann, M.; Candrian, U.; Höfelein, C.; Lüthy, J. Polymerase chain reaction (PCR): A possible alternative to immunochemical methods assuring safety and quality of food Detection of wheat contamination in non-wheat food products. *Z. Lebensm. Unters. Forsch.* **1993**, *196*, 248–251. [\[CrossRef\]](#)
14. Huang, C.; Sheth, S.; Li, M.; Ran, G.; Song, Q. Rapid and selective luminescent sensing of allergenic gluten by highly phosphorescent switch-on probe. *Talanta* **2018**, *190*, 292–297. [\[CrossRef\]](#)
15. Amaya-González, S.; de-Los-Santos-Álvarez, N.; Miranda-Ordieres, A.J.; Lobo-Castañón, M.J. Sensitive gluten determination in gluten-free foods by an electrochemical aptamer-based assay. *Anal. Bioanal. Chem.* **2015**, *407*, 6021–6029. [\[CrossRef\]](#)

16. Amaya-González, S.; de-los-Santos-Álvarez, N.; Lobo-Castañón, M.J.; Miranda-Ordieres, A.J.; Tuñón-Blanco, P. Amperometric quantification of gluten in food samples using an ELISA competitive assay and flow injection analysis. *Electroanalysis* **2011**, *23*, 108–114. [[CrossRef](#)]
17. López-López, L.; Miranda-Castro, R.; de-los-Santos-Álvarez, N.; Miranda-Ordieres, A.J.; Lobo-Castañón, M.J. Disposable electrochemical aptasensor for gluten determination in food. *Sens. Actuators B Chem.* **2017**, *241*, 522–527. [[CrossRef](#)]
18. Soler, M.; Estevez, M.C.; Moreno Mde, L.; Cebolla, A.; Lechuga, L.M. Label-free SPR detection of gluten peptides in urine for non-invasive celiac disease follow-up. *Biosens. Bioelectron.* **2016**, *79*, 158–164. [[CrossRef](#)]
19. Malvano, F.; Albanese, D.; Pilloton, R.; Di Matteo, M. A new label-free impedimetric aptasensor for gluten detection. *Food Control* **2017**, *79*, 200–206. [[CrossRef](#)]
20. Eksin, E.; Congur, G.; Erdem, A. Electrochemical assay for determination of gluten in flour samples. *Food Chem.* **2015**, *184*, 183–187. [[CrossRef](#)]
21. Chekin, F.; Singh, S.K.; Vasilescu, A.; Dhavale, V.M.; Kurungot, S.; Boukherroub, R.; Szunerits, S. Reduced Graphene Oxide Modified Electrodes for Sensitive Sensing of Gliadin in Food Samples. *ACS Sens.* **2016**, *1*, 1462–1470. [[CrossRef](#)]
22. Safavipour, M.; Kharaziha, M.; Amjadi, E.; Karimzadeh, F.; Allafchian, A. TiO₂ nanotubes/reduced GO nanoparticles for sensitive detection of breast cancer cells and photothermal performance. *Talanta* **2020**, *208*, 120369. [[CrossRef](#)] [[PubMed](#)]
23. Zhu, C.; Yang, G.; Li, H.; Du, D.; Lin, Y. Electrochemical sensors and biosensors based on nanomaterials and nanostructures. *Anal. Chem.* **2015**, *87*, 230–249. [[CrossRef](#)] [[PubMed](#)]
24. Khaliq, N.; Rasheed, M.A.; Cha, G.; Khan, M.; Karim, S.; Schmuiki, P.; Ali, G. Development of non-enzymatic cholesterol bio-sensor based on TiO₂ nanotubes decorated with Cu₂O nanoparticles. *Sens. Actuators B Chem.* **2020**, *302*, 127200. [[CrossRef](#)]
25. El-Naggar, M.E.; Shaheen, T.I.; Zaghloul, S.; El-Rafie, M.H.; Hebeish, A. Antibacterial Activities and UV Protection of the in Situ Synthesized Titanium Oxide Nanoparticles on Cotton Fabrics. *Ind. Eng. Chem. Res.* **2016**, *55*, 2661–2668. [[CrossRef](#)]
26. El-Naggar, M.E.; Hasanin, M.; Youssef, A.M.; Aldalbahi, A.; El-Newehy, M.H.; Abdelhameed, R.M. Hydroxyethyl cellulose/bacterial cellulose cryogel doped silver@titanium oxide nanoparticles: Antimicrobial activity and controlled release of Tebuconazole fungicide. *Int. J. Biol. Macromol.* **2020**, *165*, 1010–1021. [[CrossRef](#)]
27. Dumitriu, C.; Ungureanu, C.; Popescu, S.; Tofan, V.; Popescu, M.; Pirvu, C. Ti surface modification with a natural antioxidant and antimicrobial agent. *Surf. Coat. Technol.* **2015**, *276*, 175–185. [[CrossRef](#)]
28. Çiplak, Z.; Yildiz, N.; Çalimli, A. Investigation of Graphene/Ag Nanocomposites Synthesis Parameters for Two Different Synthesis Methods. *Fuller. Nanotub. Carbon Nanostructures* **2014**, *23*, 361–370. [[CrossRef](#)]
29. Karabacak, M.; Cinar, M.; Kurt, M.; Chinna babu, P.; Sundaraganesan, N. Experimental and theoretical FTIR and FT-Raman spectroscopic analysis of 1-pyrenecarboxylic acid. *Spectrochim. Acta Part A Mol. Biomol. Spectrosc.* **2013**, *114*, 509–519. [[CrossRef](#)]
30. Natu, M.V.; Sardinha, J.P.; Correia, I.J.; Gil, M.H. Controlled release gelatin hydrogels and lyophilisates with potential application as ocular inserts. *Biomed. Mater.* **2007**, *2*, 241–249. [[CrossRef](#)]
31. Su, Z.; Zhang, L.; Jiang, F.; Hong, M. Formation of crystalline TiO₂ by anodic oxidation of titanium. *Prog. Nat. Sci. Mater. Int.* **2013**, *23*, 294–301. [[CrossRef](#)]
32. Anitha, V.C.; Lee, J.-H.; Lee, J.; Narayan Banerjee, A.; Woo Joo, S.; Ki Min, B. Biofilm formation on a TiO₂ nanotube with controlled pore diameter and surface wettability. *Nanotechnology* **2015**, *26*, 065102. [[CrossRef](#)] [[PubMed](#)]
33. Miller, J.N.; Miller, J.C. *Statistics and Chemometrics for Analytical Chemistry*; Pearson/Prentice Hall: Saddle River, NJ, USA, 2005.